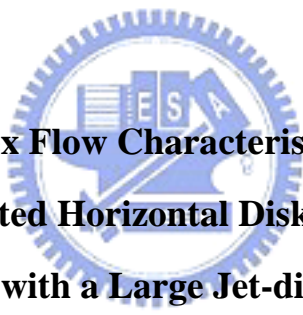


國 立 交 通 大 學

機 械 工 程 學 系

碩 士 論 文

大高度下之垂直圓柱容器中一空氣圓形噴流衝擊至一  
加熱圓盤之混合對流渦流特性研究



**Mixed Convective Vortex Flow Characteristics in a Round Jet of Air  
Impinging onto a Heated Horizontal Disk Confined in a Vertical  
Cylindrical Chamber with a Large Jet-disk Separation Distance**

研 究 生：陳 奎 銘

指 導 老 師：林 清 發 博 士

中 華 民 國 九 十 六 年 六 月

大高度下之垂直圓柱容器中一空氣圓形噴流衝擊至一加熱  
圓盤之混合對流渦流特性研究

**Mixed Convective Vortex Flow Characteristics in a Round Jet of Air  
Impinging onto a Heated Horizontal Disk Confined in a Vertical  
Cylindrical Chamber with a Large Jet-disk Separation Distance**

研究生：陳奎銘

Student : Kuei-Ming Chen

指導教授：林清發

Advisor : Tsing-Fa Lin

國立交通大學



Submitted to Institute of Mechanical Engineering

Collage of Engineering

National Chiao Tung University

In Partial Fulfillment of the Requirements

For the degree of

Master of Science

In

Mechanical Engineering

June 2007

Hsinchu, Taiwan, Republic of China

中華民國九十六年六月

# 國立交通大學

## 論文口試委員會審定書

本校 機械工程 學系碩士班 陳奎銘 君

所提論文(中文) 大高度下之垂直圓柱容器中一空氣圓形噴流衝擊  
至一加熱圓盤之混合對流渦流特性研究

(英文) Mixed Convective Vortex Flow Characteristics in a Round Jet of Air  
Impinging onto a Heated Horizontal Disk Confined in a Vertical  
Cylindrical Chamber with a Large Jet-disk Separation Distance

合於碩士資格水準、業經本委員會評審認可。

口試委員：洪道輝 何清政  
潘欽 \_\_\_\_\_  
\_\_\_\_\_

指導教授：林清發 \_\_\_\_\_

系主任：陳心舉 教授

中華民國 96 年 6 月 8 日

## 誌 謝

時光飛逝，回首在新竹這兩年來的點點滴滴，交大這充滿學術氣息的环境下似乎讓我在知識上成長茁壯許多。本論文之所以可以順利完成，首先要感謝的是指導老師 林清發 教授嚴謹及殷切的指導，使學生能培養出獨立思考、釐清並自行解決問題的能力；更在學生撰寫論文時，不辭辛勞逐字斧正文稿，在此獻上最高謝意。在研究所期間，要特別感謝謝汎鈞及羅文賢學長在實驗設備設計、架設上的協助指導，亦要感謝博士班郭威伸、賴佑民、陳尚緯、張文瑞等博士班學長在生活及課業上指導與建議，使我受益匪淺，謝謝您們。

凱文、政陞、峻樟這群不只是求學中的同學，更是生活上的好朋友。研究所之所以能在緊湊忙碌又充滿歡樂中的氣氛中度過，即是靠這些同學兼好友的夥伴們相互協助幫忙，令我永生難忘。另外也要感謝 壹龍、永龍、長志、浚圩等一群努力的學弟妹幫忙及合作，希望你們能繼續保持實驗室優良傳統，並帶著實驗室進步。

最後更要感謝父母及家人對於我無怨無悔付出及支持，使我可以無後顧之憂的專注於研究，並且可無憂無慮過求學生活。並特別要感謝女友自華的陪伴與體恤，生活最精采的部分是妳陪我渡過，不管在課業上或生活上的關心與支持使我有勇氣面對一切的困難挑戰。能與妳相處是我這輩子最大的幸福。

最後，僅以本文獻給我所關心的人和所有關心我的人。

奎銘 謹致

2007/6/30 于風城交大

# 大高度下之垂直圓柱容器中一空氣圓形噴流衝擊至一加熱圓盤之混合對流渦流特性研究

研究生：陳奎銘      指導老師：林清發博士

國立交通大學      機械工程學系

## 中文摘要

本篇論文利用實驗流場觀測方法及溫度場量測方法探討在較大的噴流到圓盤的距離對於在垂直圓柱容器中一空氣圓形噴流衝擊至一加熱圓盤的穩態及非穩態渦流結構之流場特性進行研究。由於在較大的高度下，慣性力及浮力所驅動的渦流相對的比較強烈，所以本實驗主要的研究重點是在探討噴流到圓盤的距離對於穩態及非穩態的慣性力及浮力渦流結構流場之臨界發生點與特徵，除此之外，由慣性力及浮力所造成的非穩態流場也將會註明。在本實驗研究操作範圍分別是：噴流到圓盤的距離 40~60 mm，噴流的直徑固定為 10 mm，流量變化 0~12.0 slpm，加熱圓盤與入口冷空氣間的溫度差範圍 0~25.0°C，所相對的噴流雷諾數變化為 0~1,623，相對於雷利數 0~507,348。

由流場觀測及溫度場量測可以清楚顯示噴流到圓盤的距離對於一次渦流、二次渦流、三次渦流及浮力渦流的臨界發生雷諾數有顯著的影響。其中一次渦流只有在噴流到圓盤的距離比上噴流的直徑 $HD_j$ 為 6 且非常高的浮慣比之下會消失，而二次流在 $HD_j$ 為 5 及 6 下不會出現。

除此之外，我們定義了四種典型的不穩定現象，分別是慣性力、渦流相互推擠、第一類浮力、第二類浮力所造成的不穩定渦流流場，其中第二類浮力所造成的不穩定渦流流場發生在 $HD_j$ 等於 4 到 6 且非常低的雷諾數下。而在 $HD_j$ 等於 4 時

流譜主要是由渦流相互推擠這種不穩定渦流流場所主導，而當 $HD_j$ 由 4 增加到 6 時，流譜則漸漸轉由非週期性的慣性力所造成的不穩定渦流流場主導。除此之外，當 $HD_j$ 增加時，流譜中的穩定渦流流場區域逐漸縮小。

最後，我們對由慣性力及浮力所造成的渦流及各類的渦流流場不穩定性的實驗結果做分析，求得經驗公式。



# **Mixed Convective Vortex Flow Characteristics in a Round Jet of Air Impinging onto a Heated Horizontal Disk Confined in a Vertical Cylindrical Chamber with a Large Jet-disk Separation Distance**

**Student: Kuei-Ming Chen**

**Advisor: Prof. Tsing-Fa Lin**

**Institute of Mechanical Engineering**

**National Chiao Tung University**



## **ABSTRACT**

An experiment combining flow visualization and temperature measurement is carried out in the present study to investigate how the jet-disk separation distance  $H$  affects the steady and time-dependent vortex flow resulting from a round air jet impinging onto a heated horizontal circular disk confined in a vertical cylindrical chamber when  $H$  is large. The study is motivated by the fact that at the large  $H$  the interactions between the inertia and buoyancy driven vortex rolls are relatively strong. Particular attention is paid to examining the effects of  $H$  on the onsets and characteristics of steady and time-dependent inertia and buoyancy driven vortex flows. Besides, the onsets of the inertia and buoyancy driven vortex flow instabilities affected by  $H$  will be inspected. In the present experiment three jet-disk separation distances are considered with  $H = 40.0, 50.0, \text{ and } 60.0$  mm for a fixed injection pipe diameter with  $D_j = 10.0$  mm. The jet flow rate is varied from 0 to 12.0 slpm (standard liter per minute) for the jet Reynolds number  $Re_j$  ranging from 0 to 1,623. The

temperature difference between the disk and the air injected into the chamber is varied from 0 to 25.0°C for the Rayleigh number  $Ra$  ranging from 0 to 507,348.

The results from the flow visualization and the measured temperature data clearly show the significant effects of the jet-disk separation distance on the critical  $Re_j$  for the onset of the primary, secondary and tertiary inertia-driven rolls, and the buoyancy-driven roll. The primary inertia-driven roll disappears only at a very low  $Re_j$  and at a very high buoyancy-to-inertia ratio for  $HD_j = 6$ . Besides, the secondary inertia-driven roll does not appear at larger jet-disk separation distance for  $HD_j = 5$  & 6.

Moreover, we identify four different types of vortex flow instabilities (inertia-driven, mutual roll-pushing, type-1 buoyancy-driven, and type-2 buoyancy-driven) when  $HD_j$  is varied from 1 to 6. It is noted that the type-2 buoyancy-driven vortex flow instability only occurs at very low  $Re_j$  with a large jet-disk separation distance for  $HD_j = 4$  to 6. Furthermore, the mutual roll-pushing unstable vortex flow almost occupies the flow regime map for  $HD_j = 4$  and the region dominated by the nonperiodic inertia-driven unstable vortex flow becomes larger in the flow regime map as  $HD_j$  is raised from 4 to 6. Furthermore, the region of the stable vortex flow in the flow regime map becomes smaller at increasing  $HD_j$ .

Finally, empirical correlations are proposed for the critical conditions for the onsets of the inertia and buoyancy driven vortex rolls and for the onsets of various vortex flow instabilities.



# TABLE OF CONTENTS

<b>ABSTRACT</b>	<b>i</b>
<b>TABLE OF CONTENTS</b>	<b>iii</b>
<b>LIST OF TABLES</b>	<b>v</b>
<b>LIST OF FIGURES</b>	<b>vi</b>
<b>NOMENCLATURE</b>	<b>xiv</b>
<b>CHAPTER 1 INTRODUCTION</b>	<b>1</b>
1.1 Motivation	1
1.2 Literature Review	2
1.3 Objective and Scope of Present Study	6
<b>CHAPTER 2 EXPERIMENTAL APPARATUS AND PROCEDURES</b>	<b>8</b>
2.1 Experimental Apparatus	8
2.2 Experimental Procedures	11
<b>CHAPTER 3 DIMENSIONLESS GROUPS AND UNCERTAINTY ANALYSIS</b>	<b>16</b>
3.1 Dimensionless Groups	16
3.2 Uncertainty Analysis	16

<b>CHAPTER 4</b>	<b>RESULTS AND DISCUSSION</b>	<b>20</b>
	4.1 Typical Vortex Flow Patterns	<b>21</b>
	4.2 Effects of $HD_j$ on Onsets of Inertia and Buoyancy	<b>23</b>
	Driven Vortex Rolls	
	4.3 Effects of $HD_j$ on Steady Vortex Flow Characteristics	<b>28</b>
	4.4 Effects of $HD_j$ on Vortex Flow Instabilities	<b>30</b>
	4.5 Effects of $HD_j$ on Time-Dependent Vortex Flow Characteristics	<b>38</b>
<b>CHAPTER 5</b>	<b>CONCLUDING REMARKS</b>	<b>161</b>
<b>REFERECES</b>		<b>164</b>



## LIST OF TABLES

Table 3.1	Summary of uncertainty analysis. -----	19
Table 4.1	Critical condition for appearance of the inertia-driven vortex flow ( $\Delta T=0^\circ\text{C}$ ). -----	41
Table 4.2	Critical condition for the onset of the Buoyancy-driven vortex roll for various H. -----	42
Table 4.3	Critical condition for appearance of the primary inertia-driven vortex roll at H = 60.0 mm. -----	43
Table 4.4	Critical condition for the onset of the inertia-driven time-dependent vortex flow for various H. -----	44
Table 4.5	Critical condition for the onset of the mutual roll-pushing vortex flow instability for various H. -----	45
Table 4.6	Critical condition for the onset of nonperiodic type-2 buoyancy-driven time-dependent vortex flow. -----	46



## LIST OF FIGURES

Fig. 1.1	Flow regimes associated with a circular jet impinging onto a flat plate. -----	7
Fig. 2.1	Schematic diagram of the experimental apparatus.-----	13
Fig. 2.2	The heater consists of three parts: resistance heating element, holder and insulator.-----	14
Fig. 2.3	The locations of the detection points on the upper copper plate. -----	15
Fig. 4.1	Steady vortex flow pattern in the chamber with $H = 40.0$ mm for $Re_j = 541$ ( $Q_j = 4.0$ slpm) and $Ra = 0$ ( $\Delta T = 0^\circ C$ ) : (a) side view flow photo taken at the vertical plane $\theta = 0^\circ$ & $\theta = 180^\circ$ and (b) the corresponding schematically sketched cross vortex flow. -----	47
Fig. 4.2	Vortex flow pattern in the chamber with side view flow photo taken at the vertical plane $\theta = 0^\circ$ & $\theta = 180^\circ$ and the corresponding schematically sketched cross vortex flow for $Re_j = 947$ ( $Q_j = 7.0$ slpm) and $Ra = 0$ ( $\Delta T = 0^\circ C$ ) : (a) $H = 30.0$ mm (b) $H = 50.0$ mm. -----	48
Fig. 4.3	Steady vortex flow pattern in the chamber with $H = 40.0$ mm for $Re_j = 406$ ( $Q_j = 3.0$ slpm) and $Ra = 30,065$ ( $\Delta T = 5^\circ C$ ) for (a) side view flow photo taken at the vertical plane $\theta = 0^\circ$ & $\theta = 180^\circ$ and (b) the corresponding schematically sketched cross vortex flow. -----	49
Fig. 4.4	Steady side view flow photos taken at the cross plane $\theta = 0^\circ$ & $180^\circ$ at $Q_j = 3.0$ slpm ( $Re_j = 406$ ) and $\Delta T = 5^\circ C$ for (a) $H = 20.0$ mm and (b) $H = 40.0$ mm. -----	50
Fig. 4.5	Side view flow photos taken at the cross plane $\theta = 0^\circ$ & $180^\circ$ for various jet Reynolds numbers at $Ra = 0$ ( $\Delta T = 0^\circ C$ ) for $H = 40.0$ mm. -----	51
Fig. 4.6	Steady side view flow photos taken at the cross plane $\theta = 0^\circ$ & $180^\circ$ for various $HD_j$ at $\Delta T = 0^\circ C$ ( $Ra = 0$ ) and $Q_j = 2.0$ slpm ( $Re_j = 270$ ). -----	52
Fig. 4.7	Side view flow photos taken at the cross plane $\theta = 0^\circ$ & $180^\circ$ for various jet Reynolds numbers at $Ra = 0$ ( $\Delta T = 0^\circ C$ ) for $H = 50.0$ mm. -----	53
Fig. 4.8	Side view flow photos taken at the cross plane $\theta = 0^\circ$ & $180^\circ$ for various jet Reynolds numbers at $Ra = 0$ ( $\Delta T = 0^\circ C$ ) for $H = 60.0$ mm. -----	54
Fig. 4.9	Side view flow photos taken at the cross plane for various $HD_j$ and $Re_j$ with the disk unheated ( $\Delta T = 0^\circ C$ ). -----	55
Fig. 4.10	Side view flow photos taken the cross plane $\theta = 0^\circ$ & $180^\circ$ for various jet Reynolds numbers at $Ra = 0$ ( $\Delta T = 0^\circ C$ ) for (a) $H = 40.0$ mm and (b) $H = 50.0$ mm. -----	56
Fig. 4.11	Side view flow photos taken at the cross plane $\theta = 0^\circ$ & $180^\circ$ for various $HD_j$ and $Re_j$ at $\Delta T = 5^\circ C$ . -----	57
Fig. 4.12	Side view flow photos taken at the cross plane $\theta = 0^\circ$ & $180^\circ$ for	

	$Re_j=1,623$ ( $Q_j=12.0$ slpm) with various $Ra$ at $H=30.0$ mm. -----	58
Fig. 4.13	Side view flow photos taken at the cross plane $\theta=0^\circ$ & $180^\circ$ for various $HD_j$ and $Re_j$ at $\Delta T=5^\circ C$ . -----	59
Fig. 4.14	Unsteady side view flow photos taken at the cross plane for various jet Reynolds numbers at $Ra=202,939$ ( $\Delta T=10^\circ C$ ) for $H=60.0$ mm. -----	60
Fig. 4.15	Side view flow photos taken at the cross plane $\theta=0^\circ$ & $180^\circ$ for various jet Reynolds numbers at $Ra=0$ ( $\Delta T=0^\circ C$ ) for $H=40.0$ mm. -----	61
Fig. 4.16	Side view flow photos taken at the cross plane $\theta=0^\circ$ & $180^\circ$ for various jet Reynolds numbers at $Ra=0$ ( $\Delta T=0^\circ C$ ) for (a) $H=50.0$ mm and (b) $H=60.0$ mm. -----	62
Fig. 4.17	Side view flow photos taken at the cross plane $\theta=0^\circ$ & $180^\circ$ for various jet Reynolds numbers at $\Delta T=10^\circ C$ for (a) $H=40.0$ mm, (b) $H=50.0$ mm, and (c) $H=60.0$ mm. -----	63
Fig. 4.18	Steady side view flow photos taken at the cross plane $\theta=0^\circ$ & $180^\circ$ for various $HD_j$ at $\Delta T=0^\circ C$ ( $Ra=0$ ) and $Q_j=1.0$ slpm ( $Re_j=135$ ). -----	64
Fig. 4.19	Steady side view flow photos taken at the cross plane $\theta=0^\circ$ & $180^\circ$ for various $HD_j$ at $\Delta T=0^\circ C$ ( $Ra=0$ ) and $Q_j=2.0$ slpm ( $Re_j=270$ ). -----	65
Fig. 4.20	Steady side view flow photos taken at the cross plane $\theta=0^\circ$ & $180^\circ$ for various $HD_j$ at $\Delta T=0^\circ C$ ( $Ra=0$ ) and $Q_j=3.0$ slpm ( $Re_j=406$ ). -----	66
Fig. 4.21	Steady side view flow photos taken at the cross plane $\theta=0^\circ$ & $180^\circ$ for various $HD_j$ at $\Delta T=0^\circ C$ ( $Ra=0$ ) and $Q_j=4.0$ slpm ( $Re_j=541$ ). -----	67
Fig. 4.22	Steady side view flow photos taken at the cross plane $\theta=0^\circ$ & $180^\circ$ for various $HD_j$ at $\Delta T=5^\circ C$ and $Q_j=1.0$ slpm ( $Re_j=135$ ). -----	68
Fig. 4.23	Steady side view flow photos taken at the cross plane $\theta=0^\circ$ & $180^\circ$ for various $HD_j$ at $\Delta T=5^\circ C$ and $Q_j=2.0$ slpm ( $Re_j=270$ ). -----	69
Fig. 4.24	Steady side view flow photos taken at the cross plane $\theta=0^\circ$ & $180^\circ$ for various $HD_j$ at $\Delta T=5^\circ C$ and $Q_j=3.0$ slpm ( $Re_j=406$ ). -----	70
Fig. 4.25	Steady side view flow photos taken at the cross plane $\theta=0^\circ$ & $180^\circ$ for various $HD_j$ at $\Delta T=10^\circ C$ and $Q_j=1.0$ slpm ( $Re_j=135$ ). -----	71
Fig. 4.26	Steady side view flow photos taken at the cross plane $\theta=0^\circ$ & $180^\circ$ for various $HD_j$ at $\Delta T=10^\circ C$ and $Q_j=2.0$ slpm ( $Re_j=270$ ). -----	72
Fig. 4.27	Steady side view flow photos taken at the cross plane $\theta=0^\circ$ & $180^\circ$ for various $HD_j$ at $\Delta T=15^\circ C$ and $Q_j=1.0$ slpm ( $Re_j=135$ ). -----	73
Fig. 4.28	Steady side view flow photos taken at the cross plane $\theta=0^\circ$ & $180^\circ$ for various $HD_j$ at $\Delta T=20^\circ C$ and $Q_j=1.0$ slpm ( $Re_j=135$ ). -----	74
Fig. 4.29	Steady side view flow photos taken at the cross plane $\theta=0^\circ$ & $180^\circ$ for various $HD_j$ at $\Delta T=25^\circ C$ and $Q_j=1.0$ slpm ( $Re_j=135$ ). -----	75
Fig. 4.30	Radial variation in non-dimensional steady air temperature with $Re_j=135$ ( $Q_j=1.0$ slpm) and $\Delta T=5.0^\circ C$ at $Z=0.5$ on the vertical plane $\theta=0^\circ$ for	

	HD <sub>j</sub> = 4, 5 , and 6.-----	76
Fig. 4.31	Steady side view flow photos taken at the cross plane $\theta=0^\circ$ & $180^\circ$ for various jet Reynolds numbers at Ra=30,065 ( $\Delta T=5^\circ\text{C}$ ) for H = 40.0 mm. -----	77
Fig. 4.32	Steady side view flow photos taken at the cross plane $\theta=0^\circ$ & $180^\circ$ for various jet Reynolds numbers at Ra=60,130 ( $\Delta T=10^\circ\text{C}$ ) for H = 40.0 mm. -----	78
Fig. 4.33	Steady side view flow photos taken at the cross plane $\theta=0^\circ$ & $180^\circ$ for various jet Reynolds numbers at Ra=90,195 ( $\Delta T=15^\circ\text{C}$ ) for H = 40.0 mm. -----	79
Fig. 4.34	Steady side view flow photos taken at the cross plane $\theta=0^\circ$ & $180^\circ$ for various jet Reynolds numbers at Ra=120,260 ( $\Delta T=20^\circ\text{C}$ ) for H = 40.0 mm. -----	80
Fig. 4.35	Steady side view flow photos taken at the cross plane $\theta=0^\circ$ & $180^\circ$ for various jet Reynolds numbers at Ra=58,721 ( $\Delta T=5^\circ\text{C}$ ) for H = 50.0 mm. -----	81
Fig. 4.36	Steady side view flow photos taken at the cross plane $\theta=0^\circ$ & $180^\circ$ for various jet Reynolds numbers at Ra=117,442 ( $\Delta T=10^\circ\text{C}$ ) for H = 50.0 mm. -----	82
Fig. 4.37	Steady side view flow photos taken at the cross plane $\theta=0^\circ$ & $180^\circ$ for various jet Reynolds numbers at Ra=101,470 ( $\Delta T=5^\circ\text{C}$ ) for H = 60.0 mm. -----	83
Fig. 4.38	Steady side view flow photos taken at the cross plane $\theta=0^\circ$ & $180^\circ$ for various temperature difference at Re <sub>j</sub> =135 (Q <sub>j</sub> =1.0slpm) and H = 40.0 mm. -----	84
Fig. 4.39	Steady side view flow photos taken at the cross plane $\theta=0^\circ$ & $180^\circ$ for various temperature difference at Re <sub>j</sub> =135 (Q <sub>j</sub> =1.0slpm) and H = 50.0 mm. -----	85
Fig. 4.40	Side view flow photos taken at the cross plane $\theta=0^\circ$ & $180^\circ$ for various jet Reynolds numbers at Ra=0 ( $\Delta T=0^\circ\text{C}$ ) and H = 20.0 mm. -----	86
Fig. 4.41	Side view flow photos taken at the cross plane $\theta=0^\circ$ & $180^\circ$ for various jet Reynolds numbers at Ra=7,520 ( $\Delta T=10^\circ\text{C}$ ) and H = 20.0 mm.-----	87
Fig. 4.42	Side view flow photos taken at the cross plane $\theta=0^\circ$ & $180^\circ$ for various jet Reynolds numbers at Ra=0 ( $\Delta T=0^\circ\text{C}$ ) and H = 30.0 mm. -----	88
Fig. 4.43	Side view flow photos taken at the cross plane $\theta=0^\circ$ & $180^\circ$ for various jet Reynolds numbers at Ra=0 ( $\Delta T=0^\circ\text{C}$ ) and H = 40.0 mm. -----	89
Fig. 4.44	Side view flow photos taken at the cross plane $\theta=0^\circ$ & $180^\circ$ for various jet Reynolds numbers at Ra=0 ( $\Delta T=0^\circ\text{C}$ ) and H = 50.0 mm. -----	90
Fig. 4.45	Side view flow photos taken at the cross plane $\theta=0^\circ$ & $180^\circ$ for various jet Reynolds numbers at Ra=0 ( $\Delta T=0^\circ\text{C}$ ) fo H = 60.0 mm. -----	91
Fig. 4.46	Unsteady side view flow photos taken at the cross plane $\theta=0^\circ$ & $180^\circ$ for	

	various jet Reynolds numbers at $Ra=60,160$ ( $\Delta T=10^\circ C$ ) for $H = 40.0$ mm. -----	92
Fig. 4.47	Unsteady side view flow photos taken at the cross plane $\theta=0^\circ$ & $180^\circ$ for various jet Reynolds numbers at $Ra=90,195$ ( $\Delta T=15^\circ C$ ) for $H = 40.0$ mm. -----	93
Fig. 4.48	Unsteady side view flow photos taken at the cross plane $\theta=0^\circ$ & $180^\circ$ for various jet Reynolds numbers at $Ra=120,260$ ( $\Delta T=20^\circ C$ ) for $H = 40.0$ mm. -----	94
Fig. 4.49	Side view flow photos taken at the cross plane $\theta=0^\circ$ & $180^\circ$ for various jet Reynolds numbers at $Ra=117,442$ ( $\Delta T=10^\circ C$ ) for $H = 50.0$ mm. -----	95
Fig. 4.50	Unsteady side view flow photos taken at the cross plane $\theta=0^\circ$ & $180^\circ$ for various jet Reynolds numbers at $Ra=176,162$ ( $\Delta T=15^\circ C$ ) for $H = 50.0$ mm. -----	96
Fig. 4.51	Unsteady side view flow photos taken at the cross plane $\theta=0^\circ$ & $180^\circ$ for various jet Reynolds numbers at $Ra=234,883$ ( $\Delta T=20^\circ C$ ) for $H = 50.0$ mm. -----	97
Fig. 4.52	Unsteady side view flow photos taken at the cross plane $\theta=0^\circ$ & $180^\circ$ for various jet Reynolds numbers at $Ra=293,604$ ( $\Delta T=25^\circ C$ ) for $H = 50.0$ mm. -----	98
Fig. 4.53	Unsteady side view flow photos taken at the cross plane $\theta=0^\circ$ & $180^\circ$ for various jet Reynolds numbers at $Ra=202,939$ ( $\Delta T=10^\circ C$ ) fo $H = 60.0$ mm. -----	99
Fig. 4.54	Unsteady side view flow photos taken at the cross plane $\theta=0^\circ$ & $180^\circ$ for various jet Reynolds numbers at $Ra=304,409$ ( $\Delta T=15^\circ C$ ) fo $H = 60.0$ mm. -----	100
Fig. 4.55	Unsteady side view flow photos taken at the cross plane $\theta=0^\circ$ & $180^\circ$ for various jet Reynolds numbers at $Ra=405,878$ ( $\Delta T=20^\circ C$ ) fo $H = 60.0$ mm. -----	101
Fig. 4.56	Unsteady side view flow photos taken at the cross plane $\theta=0^\circ$ & $180^\circ$ for various jet Reynolds numbers at $Ra=507,348$ ( $\Delta T=25^\circ C$ ) fo $H = 60.0$ mm. -----	102
Fig. 4.57	Time-periodic vortex flow for $H = 20.0$ mm and $Ra = 0$ ( $\Delta T=0^\circ C$ ) at $Re_j=839$ ( $Q_j=6.2$ slpm) illustrated by side view flow photos taken at the cross plane $\theta=0^\circ$ & $180^\circ$ at selected time instants in a typical periodic cycle ( $t_p = 1.45$ sec). -----	103
Fig. 4.58	Time-periodic vortex flow for $H = 20.0$ mm and $Ra = 18,790$ ( $\Delta T=25^\circ C$ ) at $Re_j=1,028$ ( $Q_j=7.6$ slpm) illustrated by side view flow photos taken at the cross plane $\theta=0^\circ$ & $180^\circ$ at selected time instants in a typical periodic cycle ( $t_p = 1.58$ sec).-----	104

Fig. 4.59	Time-periodic vortex flow for $H = 40.0$ mm and $Ra = 0$ ( $\Delta T = 0^\circ\text{C}$ ) at $Re_j = 676$ ( $Q_j = 5.0$ slpm) illustrated by side view flow photos taken at the cross plane $\theta = 0^\circ$ & $180^\circ$ at selected time instants in a typical periodic cycle ( $t_p = 4.3$ sec).-----	105
Fig. 4.60	Nonperiodic vortex flow for $H = 40.0$ mm and $Ra = 60,130$ ( $\Delta T = 10^\circ\text{C}$ ) at $Re_j = 1,352$ ( $Q_j = 10.0$ slpm) illustrated by side view flow photos taken at the cross plane $\theta = 0^\circ$ & $180^\circ$ at selected time instants.-----	106
Fig. 4.61	Side view flow photos taken at the cross plane $\theta = 0^\circ$ & $180^\circ$ for various jet Reynolds numbers at $Ra = 30,065$ ( $\Delta T = 5^\circ\text{C}$ ) and $H = 40.0$ mm.-----	107
Fig. 4.62	Side view flow photos taken at the cross plane $\theta = 0^\circ$ & $180^\circ$ for various jet Reynolds numbers at $Ra = 60,130$ ( $\Delta T = 10^\circ\text{C}$ ) and $H = 40.0$ mm.-----	108
Fig. 4.63	Side view flow photos taken at the cross plane $\theta = 0^\circ$ & $180^\circ$ for various jet Reynolds numbers at $Ra = 90,195$ ( $\Delta T = 15^\circ\text{C}$ ) and $H = 40.0$ mm.-----	109
Fig. 4.64	Side view flow photos taken at the cross plane $\theta = 0^\circ$ & $180^\circ$ for various jet Reynolds numbers at $Ra = 120,320$ ( $\Delta T = 20^\circ\text{C}$ ) and $H = 40.0$ mm.-----	110
Fig. 4.65	Side view flow photos taken at the cross plane $\theta = 0^\circ$ & $180^\circ$ for various jet Reynolds numbers at $Ra = 150,325$ ( $\Delta T = 25^\circ\text{C}$ ) and $H = 40.0$ mm.-----	111
Fig. 4.66	Side view flow photos taken at the cross plane $\theta = 0^\circ$ & $180^\circ$ for various temperature difference at $Re_j = 270$ ( $Q_j = 2.0$ slpm) and $H = 40.0$ mm.-----	112
Fig. 4.67	Side view flow photos taken at the cross plane $\theta = 0^\circ$ & $180^\circ$ for various temperature difference at $Re_j = 406$ ( $Q_j = 3.0$ slpm) and $H = 40.0$ mm.-----	113
Fig. 4.68	Side view flow photos taken at the cross plane $\theta = 0^\circ$ & $180^\circ$ for various jet Reynolds numbers at $Ra = 58,721$ ( $\Delta T = 5^\circ\text{C}$ ) for $H = 50.0$ mm.-----	114
Fig. 4.69	Side view flow photos taken at the cross plane $\theta = 0^\circ$ & $180^\circ$ for various jet Reynolds numbers at $Ra = 117,442$ ( $\Delta T = 10^\circ\text{C}$ ) for $H = 50.0$ mm.-----	115
Fig. 4.70	Side view flow photos taken at the cross plane $\theta = 0^\circ$ & $180^\circ$ for various jet Reynolds numbers at $Ra = 176,162$ ( $\Delta T = 15^\circ\text{C}$ ) for $H = 50.0$ mm.-----	116
Fig. 4.71	Side view flow photos taken at the cross plane $\theta = 0^\circ$ & $180^\circ$ for various temperature difference at $Re_j = 270$ ( $Q_j = 2.0$ slpm) and $H = 50.0$ mm.-----	117
Fig. 4.72	Side view flow photos taken at the cross plane $\theta = 0^\circ$ & $180^\circ$ for various jet Reynolds numbers at $Ra = 101,470$ ( $\Delta T = 5^\circ\text{C}$ ) fo $H = 60.0$ mm.-----	118
Fig. 4.73	Time-periodic vortex flow illustrated by side view flow photos taken at the cross plane $\theta = 0^\circ$ & $180^\circ$ at selected time instants for $H = 40$ mm and $Ra = 90,195$ ( $\Delta T = 15^\circ\text{C}$ ) at $Re_j = 676$ ( $Q_j = 5.0$ slpm) with $t_p = 1.82$ sec.-----	119
Fig. 4.74	Time-periodic vortex flow for $H = 20.0$ mm and $Ra = 11,270$ ( $\Delta T = 15.0^\circ\text{C}$ ) at $Re_j = 135$ ( $Q_j = 1.0$ slpm) illustrated by side view flow photos taken at the vertical plane $\theta = 0^\circ$ & $180^\circ$ at selected time instants.-----	120
Fig. 4.75	Nonperiodic vortex flow for $H = 40.0$ mm and $Ra = 90,195$ ( $\Delta T = 15^\circ\text{C}$ ) at $Re_j = 41$ ( $Q_j = 0.3$ slpm) illustrated by side view flow photos taken at	



	the cross plane $\theta=0^\circ$ & $180^\circ$ at selected time instants.-----	121
Fig. 4.76	Nonperiodic vortex flow for $H = 40.0$ mm and $Ra = 90,195$ ( $\Delta T=15^\circ\text{C}$ ) at $Re_j=27$ ( $Q_j=0.2$ slpm) illustrated by side view flow photos taken at the cross plane $\theta=0^\circ$ & $180^\circ$ at selected time instants.-----	122
Fig. 4.77	Nonperiodic vortex flow for $H = 40.0$ mm and $Ra = 120,260$ ( $\Delta T=20^\circ\text{C}$ ) at $Re_j=41$ ( $Q_j=0.3$ slpm) illustrated by side view flow photos taken at the cross plane $\theta=0^\circ$ & $180^\circ$ at selected time instants.-----	123
Fig. 4.78	Nonperiodic vortex flow for $H = 50.0$ mm and $Ra = 58,721$ ( $\Delta T=5^\circ\text{C}$ ) at $Re_j=54$ ( $Q_j=0.4$ slpm) illustrated by side view flow photos taken at the cross plane $\theta=0^\circ$ & $180^\circ$ at selected time instants.-----	124
Fig. 4.79	Nonperiodic vortex flow for $H = 50.0$ mm and $Ra = 58,721$ ( $\Delta T=5^\circ\text{C}$ ) at $Re_j=68$ ( $Q_j=0.5$ slpm) illustrated by side view flow photos taken at the cross plane $\theta=0^\circ$ & $180^\circ$ at selected time instants.-----	125
Fig. 4.80	Nonperiodic vortex flow for $H = 50.0$ mm and $Ra = 117,442$ ( $\Delta T=10^\circ\text{C}$ ) at $Re_j=68$ ( $Q_j=0.5$ slpm) illustrated by side view flow photos taken at the cross plane $\theta=0^\circ$ & $180^\circ$ at selected time instants.-----	126
Fig. 4.81	Nonperiodic vortex flow for $H = 60.0$ mm and $Ra = 202,939$ ( $\Delta T=10^\circ\text{C}$ ) at $Re_j=68$ ( $Q_j=0.5$ slpm) illustrated by side view flow photos taken at the cross plane $\theta=0^\circ$ & $180^\circ$ at selected time instants.-----	127
Fig. 4.82	Side view flow photos taken at the cross plane $\theta=0^\circ$ & $180^\circ$ for various jet Reynolds numbers at $Ra=30,065$ ( $\Delta T=5^\circ\text{C}$ ) for $H = 40.0$ mm.-----	128
Fig. 4.83	Side view flow photos taken the cross plane $\theta=0^\circ$ & $180^\circ$ for various jet Reynolds numbers at $Ra=60,130$ ( $\Delta T=10^\circ\text{C}$ ) for $H = 40.0$ mm.-----	129
Fig. 4.84	Side view flow photos taken at the cross plane $\theta=0^\circ$ & $180^\circ$ for various jet Reynolds numbers at $Ra=90,195$ ( $\Delta T=15^\circ\text{C}$ ) for $H = 40.0$ mm.-----	130
Fig. 4.85	Side view flow photos taken at the cross plane $\theta=0^\circ$ & $180^\circ$ for various jet Reynolds numbers at $Ra=120,260$ ( $\Delta T=20^\circ\text{C}$ ) fo $H = 40.0$ mm.-----	131
Fig. 4.86	Side view flow photos taken at the cross plane $\theta=0^\circ$ & $180^\circ$ for various jet Reynolds numbers at $Ra=58,721$ ( $\Delta T=5^\circ\text{C}$ ) for $H = 50.0$ mm.-----	132
Fig. 4.87	Side view flow photos taken at the cross plane $\theta=0^\circ$ & $180^\circ$ for various jet Reynolds numbers at $Ra=117,442$ ( $\Delta T=10^\circ\text{C}$ ) for $H = 50.0$ mm.-----	133
Fig. 4.88	Side view flow photos taken at the cross plane $\theta=0^\circ$ & $180^\circ$ for various jet Reynolds numbers at $Ra=176,162$ ( $\Delta T=15^\circ\text{C}$ ) for $H = 50.0$ mm.-----	134
Fig. 4.89	Side view flow photos taken at the cross plane $\theta=0^\circ$ & $180^\circ$ for various jet Reynolds numbers at $Ra=234,883$ ( $\Delta T=20^\circ\text{C}$ ) for $H = 50.0$ mm.-----	135
Fig. 4.90	Side view flow photos taken at the cross plane $\theta=0^\circ$ & $180^\circ$ for various jet Reynolds numbers at $Ra=293,604$ ( $\Delta T=25^\circ\text{C}$ ) for $H = 50.0$ mm.-----	136
Fig. 4.91	Side view flow photos taken at the cross plane $\theta=0^\circ$ & $180^\circ$ for various	

	jet Reynolds numbers at $Ra=101,470$ ( $\Delta T=5^{\circ}C$ ) for $H = 60.0$ mm. -----	137
Fig. 4.92	Side view flow photos taken at the cross plane $\theta=0^{\circ}$ & $180^{\circ}$ for various jet Reynolds numbers at $Ra=202,939$ ( $\Delta T=10^{\circ}C$ ) for $H = 60.0$ mm.-----	138
Fig. 4.93	Side view flow photos taken at the cross plane $\theta=0^{\circ}$ & $180^{\circ}$ for various jet Reynolds numbers at $Ra=304,409$ ( $\Delta T=15^{\circ}C$ ) for $H = 60.0$ mm.-----	139
Fig. 4.94	Side view flow photos taken at the cross plane $\theta=0^{\circ}$ & $180^{\circ}$ for various jet Reynolds numbers at $Ra=405,878$ ( $\Delta T=20^{\circ}C$ ) for $H = 60.0$ mm.-----	140
Fig. 4.95	Side view flow photos taken at the cross plane $\theta=0^{\circ}$ & $180^{\circ}$ for various jet Reynolds numbers at $Ra=507,348$ ( $\Delta T=25^{\circ}C$ ) for $H = 60.0$ mm.-----	141
Fig. 4.96	Flow regime map delineating the temporal state of the vortex flow for $H = 40.0$ mm.-----	142
Fig. 4.97	Flow regime map delineating the temporal state of the vortex flow for $H = 50.0$ mm.-----	143
Fig. 4.98	Flow regime map delineating the temporal state of the vortex flow for $H = 60.0$ mm.-----	144
Fig. 4.99	Flow regime map delineating the temporal state of the vortex flow for $H = 10.0$ mm.-----	145
Fig. 4.100	Flow regime map delineating the temporal state of the vortex flow for $H = 20.0$ mm.-----	146
Fig. 4.101	Flow regime map delineating the temporal state of the vortex flow for $H = 30.0$ mm.-----	147
Fig. 4.102	Time-periodic vortex flow for $H = 30.0$ mm and $Ra = 38,051$ ( $\Delta T=15^{\circ}C$ ) at $Re_j=676$ ( $Q_j=5.0$ slpm) illustrated by side view flow photos taken at the cross plane $\theta=0^{\circ}$ & $180^{\circ}$ at selected time instants in a typical periodic cycle ( $t_p = 1.43$ sec).-----	148
Fig. 4.103	Time-periodic vortex flow for $H = 40.0$ mm and $Ra = 90,195$ ( $\Delta T=15^{\circ}C$ ) at $Re_j=676$ ( $Q_j=5.0$ slpm) illustrated by side view flow photos taken at the cross plane $\theta=0^{\circ}$ & $180^{\circ}$ at selected time instants in a typical periodic cycle ( $t_p = 1.82$ sec).-----	149
Fig. 4.104	Time-periodic vortex flow for $H = 50.0$ mm and $Ra = 176,162$ ( $\Delta T=15^{\circ}C$ ) at $Re_j=676$ ( $Q_j=5.0$ slpm) illustrated by side view flow photos taken at the cross plane $\theta=0^{\circ}$ & $180^{\circ}$ at selected time instants in a typical periodic cycle ( $t_p = 2.17$ sec).-----	150
Fig. 4.105	Nonperiodic vortex flow for $H = 60.0$ mm and $Ra = 304,409$ ( $\Delta T=15^{\circ}C$ ) at $Re_j=676$ ( $Q_j=5.0$ slpm) illustrated by side view flow photos taken at the cross plane $\theta=0^{\circ}$ & $180^{\circ}$ at selected time instants in a typical periodic cycle. -----	151
Fig. 4.106	The time records of non-dimensional air temperature for	

Ra=90,195( $\Delta T = 15.0^\circ\text{C}$ ) and  $Re_j=676$  ( $Q_j=5.0$  slpm) with  $H=40.0$  mm measured at selected locations on the vertical plane  $\theta = 0^\circ$  at  $Z = 0.67$  for  $R = r/R_c =$  (a) 0.17, (b) 0.45, (c) 0.62, (d)0.76, and (e) 0.96 ( $t_p=1.82$  sec).----- 152

Fig. 4.107 The time records of non-dimensional air temperature and the corresponding power spectrum densities for Ra=90,195 ( $\Delta T = 15.0^\circ\text{C}$ ) and  $Re_j=676$  ( $Q_j=5.0$  slpm) with  $H=40.0$  mm measured at selected locations on the vertical plane  $\theta = 0^\circ$  at  $Z = 0.67$  fo  $R = r/R_c =$  (a)0.45, (b)0.62, (c)0.76,and (d)0.96 ( $t_p=1.82$  sec).----- 153

Fig. 4.108 The time records of non-dimensional air temperature and the corresponding power spectrum densities for  $\Delta T = 15.0^\circ\text{C}$  and  $Re_j=676$  ( $Q_j=5.0$  slpm) with measured at selected locations on the vertical plane  $\theta = 0^\circ$  at  $Z = 0.67$  and  $R = r/R_c = 0.62$  for various  $HD_j =$  (a)4, (b)5, and (c)6.----- 154

Fig. 4.109 The time records of non-dimensional air temperature for Ra=176.162( $\Delta T = 15.0^\circ\text{C}$ ) and  $Re_j=1,488$  ( $Q_j=11.0$  slpm) with  $H=50.0$  mm measured at selected locations on the vertical plane  $\theta = 0^\circ$  at  $Z = 0.67$  for  $R = r/R_c =$  (a) 0.34, (b) 0.62, and (c) 0.96.----- 155

Fig. 4.110 The time records of non-dimensional air temperature for  $\Delta T = 15.0^\circ\text{C}$  and  $Re_j=1,488$  ( $Q_j=11.0$  slpm) with measured at selected locations on the vertical plane  $\theta = 0^\circ$  at  $Z = 0.67$  and  $R = r/R_c = 0.62$  for  $HD_j =$  (a)4, (b)5, and (c)6.----- 156

Fig. 4.111 The time records of non-dimensional air temperature for  $\Delta T = 20.0^\circ\text{C}$  and Ra=234,883 at  $H = 50.0$  mm with measured at selected locations on the vertical plane  $\theta = 0^\circ$  at  $Z = 0.67$  and  $R = r/R_c = 0.89$  for  $Re_j =$  (a) 1,190, (b) 1,352, (c) 1,488, and (d) 1,623.----- 157

Fig. 4.112 The time records of non-dimensional air temperature for Ra=176,162 ( $\Delta T = 15.0^\circ\text{C}$ ) and  $Re_j=47$  ( $Q_j=0.3$  slpm) with  $H=50.0$  mm measured at selected locations on the vertical plane  $\theta = 0^\circ$  at  $Z = 0.33$  for various  $R = r/R_c =$  (a) 0.07, (b) 0.17, (c) 0.48, and (d) 0.79.----- 158

Fig. 4.113 The time records of non-dimensional air temperature for  $\Delta T = 15.0^\circ\text{C}$  and  $Re_j=47(Q_j=0.3$  slpm) with measured at selected locations on the vertical plane  $\theta = 0^\circ$  at  $Z = 0.33$  and  $R = r/R_c = 0.17$  for  $HD_j =$  (a)4, (b)5, and (c)6.----- 159

Fig. 4.114 The time records of non-dimensional air temperature for  $\Delta T = 20.0^\circ\text{C}$  and Ra=234,883 at  $H = 50.0$  mm with measured at selected locations on the vertical plane  $\theta = 0^\circ$  at  $Z = 0.33$  and  $R = r/R_c = 0.17$  for  $Re_j =$  (a) 135, (b) 108, (c) 68, and (d) 27.----- 160

## NONMENCLATURE

$D_j$	Diameter of jet at the injection pipe exit (mm)
$D_w$	Diameter of disk (mm)
$Gr$	Grashof number, $g\beta\Delta TH^3/\nu^2$
$g$	Gravitational acceleration ( $m/s^2$ )
$H$	Jet-to-disk separation distance (mm)
$HD_j$	Ratio of the jet-disk separation distance to the jet diameter, $H/D_j$
$Q_j$	Jet flow rate (Standard Liter per Minute, slpm)
$r, \theta, z$	Dimensional coordinates in cylindrical coordinate system
$R, \Theta, Z$	Dimensionless coordinates $r/R_c, \theta/360^\circ, z/H$
$Ra$	Rayleigh number, $g\beta\Delta TH^3/\alpha\nu$
$R_c$	Radius of cylindrical chamber (mm)
$Re_j$	Jet Reynolds number, $\bar{V}_j D_j / \nu$
$Re_w$	Local Reynolds number of the flow in the wall-jet region, $\bar{u}H / \nu$
$Re_{we}$	Local Reynolds number of the flow in the wall-jet region at disk edge, $\bar{u}_{we} H / \nu$
$R_w$	Radius of disk (mm)
$T_a$	Ambient Temperature ( $^\circ C$ )
$T_f$	Temperature of the heated disk ( $^\circ C$ )
$T_j$	Temperature of jet at the injection pipe exit ( $^\circ C$ )
$t$	Time (sec)
$\bar{u}$	Average radial velocity of the flow in the wall-jet region, $Q_j / (2\pi r H)$
$\bar{u}_{we}$	Average radial velocity of the flow in the wall-jet region at disk

edge,  $Q_j/(2\pi R_w H)$

$\bar{V}_j$  Average velocity of the air jet at the injection pipe exit (m/s)

### Greek symbols

$\alpha$  Thermal diffusivity ( $\text{m}^2/\text{s}$ )

$\beta$  Thermal expansion coefficient (1/K)

$\Delta T$  Temperature difference between the heated disk and the air injected into the chamber ( $^\circ\text{C}$ )

$\nu$  Kinematic viscosity ( $\text{m}^2/\text{s}$ )

$\Phi$  Non-dimensional temperature,  $(T - T_j)/(T_r - T_j)$

$\rho$  Density ( $\text{kg}/\text{m}^3$ )

$\mu$  Dynamic viscosity ( $\text{kg}/\text{ms}$ )

$k$  Thermal conductivity ( $\text{W}/\text{m}^\circ\text{C}$ )

